

Supporting Information Available

Valence-tautomeric infinite coordination polymer nanoparticles for encapsulation of Rhodamine B and its potential application for colorimetric and fluorescent dual mode sensing of hypochlorite

Xiaolei Zhang^a, Jingjing Deng^{a*}, Guoyue Shi^b, Tianshu Zhou^{a*}

^aSchool of Ecological and Environmental Sciences, East China Normal University, 500 Dongchuan Road, Shanghai 200241, China

^bDepartment of Chemistry, East China Normal University, 500 Dongchuan Road, Shanghai 200241, China.

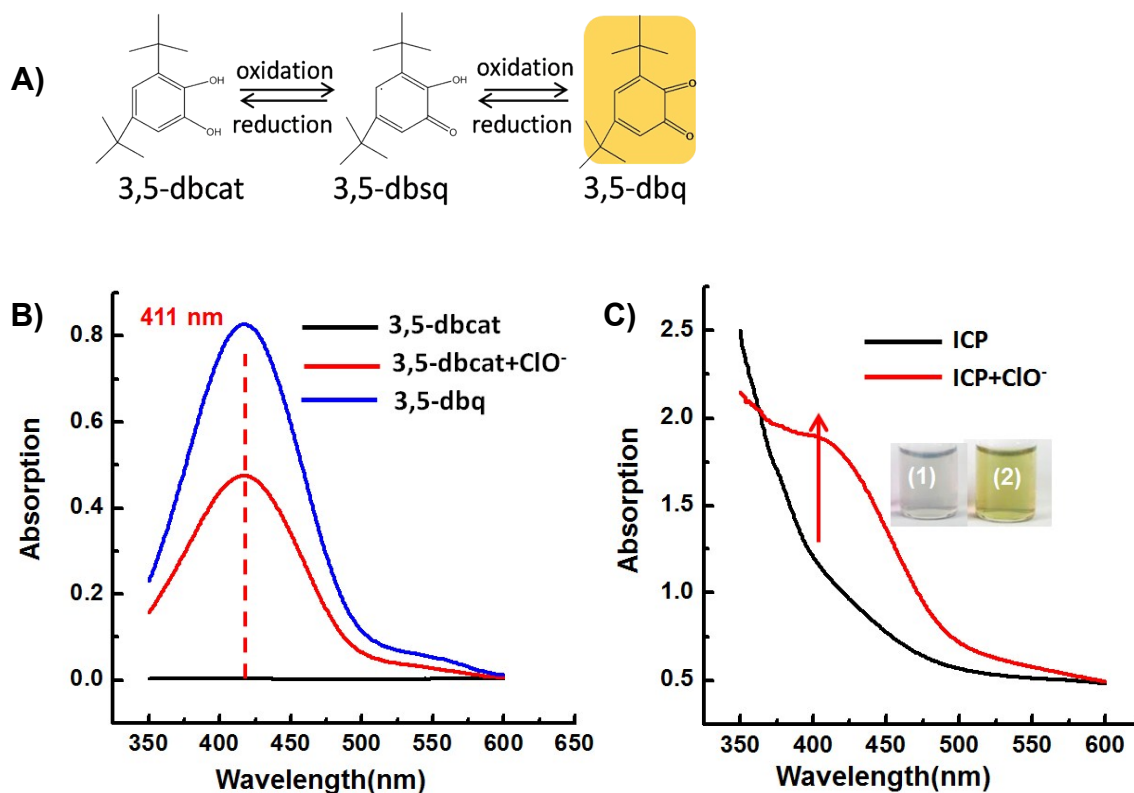


Figure S1 A) Redox reactions of redox-active ligands(3,5-dbcat and 3,5-dbsq). B) UV-Vis spectra of the 3,5-dbcat (20 $\mu\text{g}/\text{mL}$, black curve), 3,5-dbcat with the addition of ClO^- (400 μM , red curve), 3,5-dbq (blue curve) in 2 mL PBS buffer (2 mM, pH 7.0). C) UV-Vis spectra of $\{\text{Co}(3,5\text{-dbsq})(3,5\text{-dbcats})\}$ nanoparticles (0.8 mg) dispersed in 2 mL PBS buffer without (black curve) and with (red curve) the addition of 400 μM ClO^- . Inset: Photographs of ICP nanoparticles without (vial 1) and with (vial 2) the addition of 400 μM ClO^- .

As shown in Figure S1A, the 3,5-dbq (quinone molecules) undergo two-step redox reactions. The addition of ClO^- into PBS buffer containing 3,5-dbcat, leading to an increase at 411 nm (Figure S1B, from black curve to red curve). To verify the new absorbance peak, the UV-Vis spectra of 3,5-dbq was detected (blue curve). As depicted in Fig. S1B, the new absorbance peak at 411 nm belongs to 3,5-dbq, which was oxidized from 3,5-dbcat. As shown in Figure S1C, the addition of ClO^- into PBS buffer containing $\{\text{Co}(3,5\text{-dbsq})(3,5\text{-dbcats})\}$ ICP nanoparticles obviously lead to a color change of the dispersion from gray to yellow, accompany with the production of A_{411} . This phenomenon could be due to the oxidation of ClO^- convert the redox-active ligand into 3,5-dbq, leading to the increase of A_{411} .

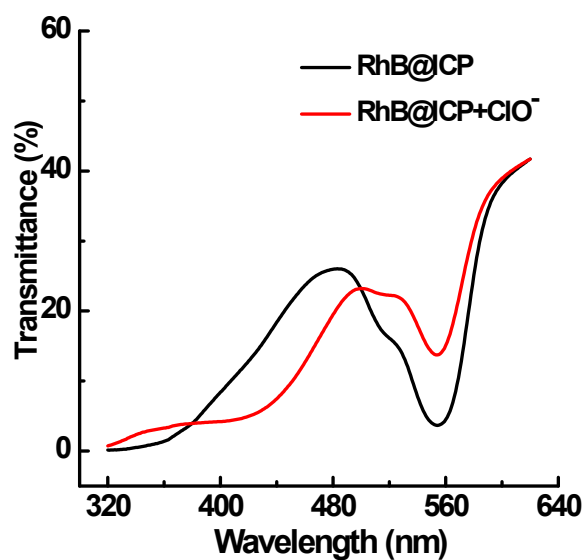


Figure S2. Transmittance spectra of RhB@{Co(3,5-dbsq)(3,5-dbcac)(bix)} nanoparticles without (black curve) and with the presence of ClO⁻ (400 μ M, red curve).

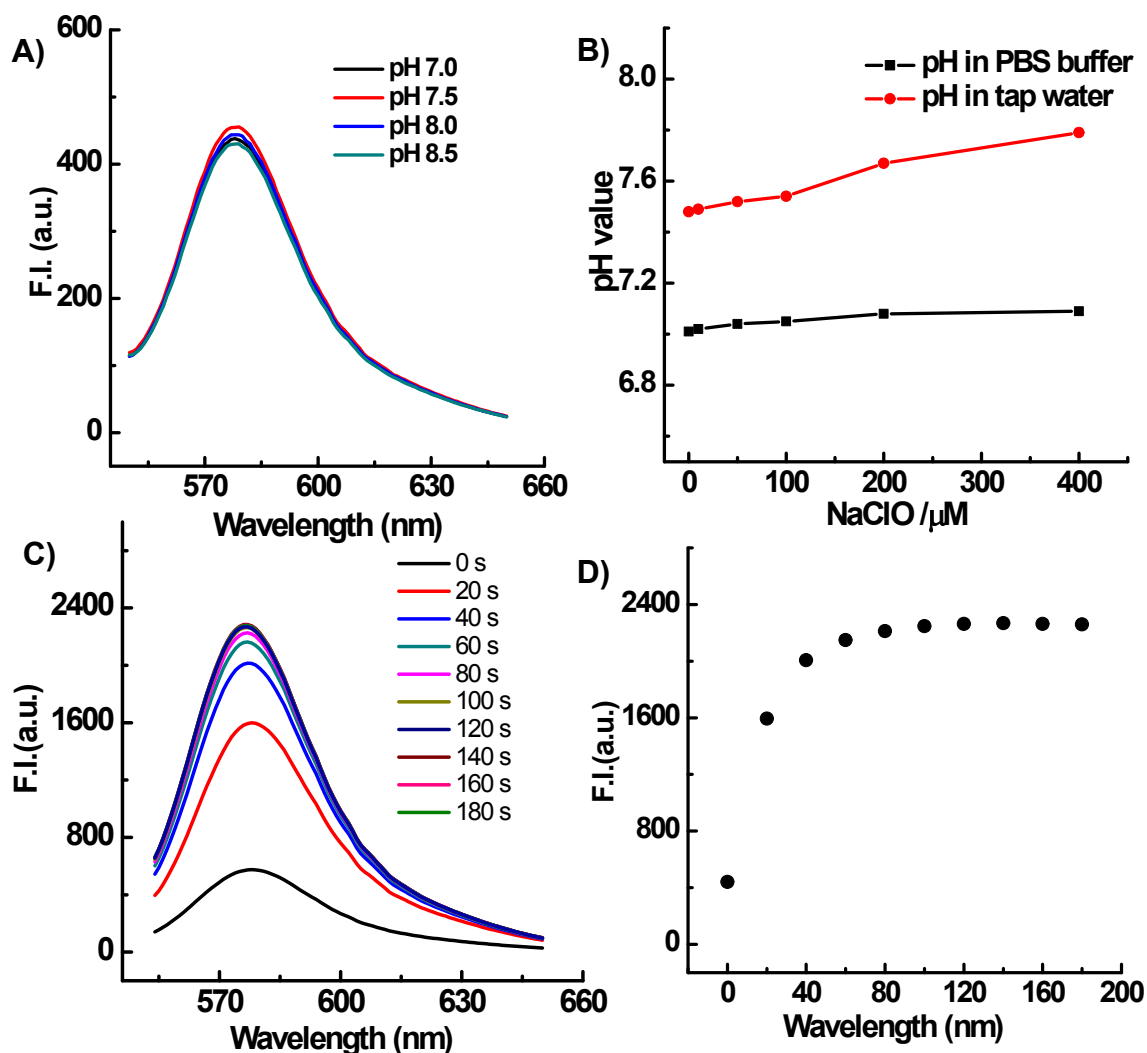


Figure S3 A) The fluorescent emission spectra of RhB@Co(3,5-dbsq)(3,5-dbcate)(bix) nanoparticles in different PBS buffer (pH value from 7.0 to 8.5). B) The pH value of RhB@Co(3,5-dbsq)(3,5-dbcate)(bix) nanoparticles in PBS buffer and tap water with the presence of ClO⁻ (from 0 μM to 400 μM). C) The time course of fluorescent emission spectra of RhB@Co(3,5-dbsq)(3,5-dbcate)(bix) nanoparticles with the addition of 400 μM ClO⁻ (λ_x=535 nm). D) The fluorescent intensity of RhB@Co(3,5-dbsq)(3,5-dbcate)(bix) nanoparticles with the addition of 400 μM ClO⁻ (λ_x=535 nm) as a function of time course.

As demonstrated in Figure S3 A, the RhB@Co(3,5-dbsq)(3,5-dbcate)(bix) nanoparticles in PBS buffer with different pH value from 7.0 to 8.5 did not result in an obvious change in the fluorescent intensity. Figure R3 B shows that the pH range of different concentration of ClO⁻ in PBS buffer was around 7.0 (from 7.01 to 7.09) and the pH range of different concentration of hypochlorite in tap water was from 7.48 to 7.79. Thus the different concentration of ClO⁻ induced the slight pH change did not affect our measurement.

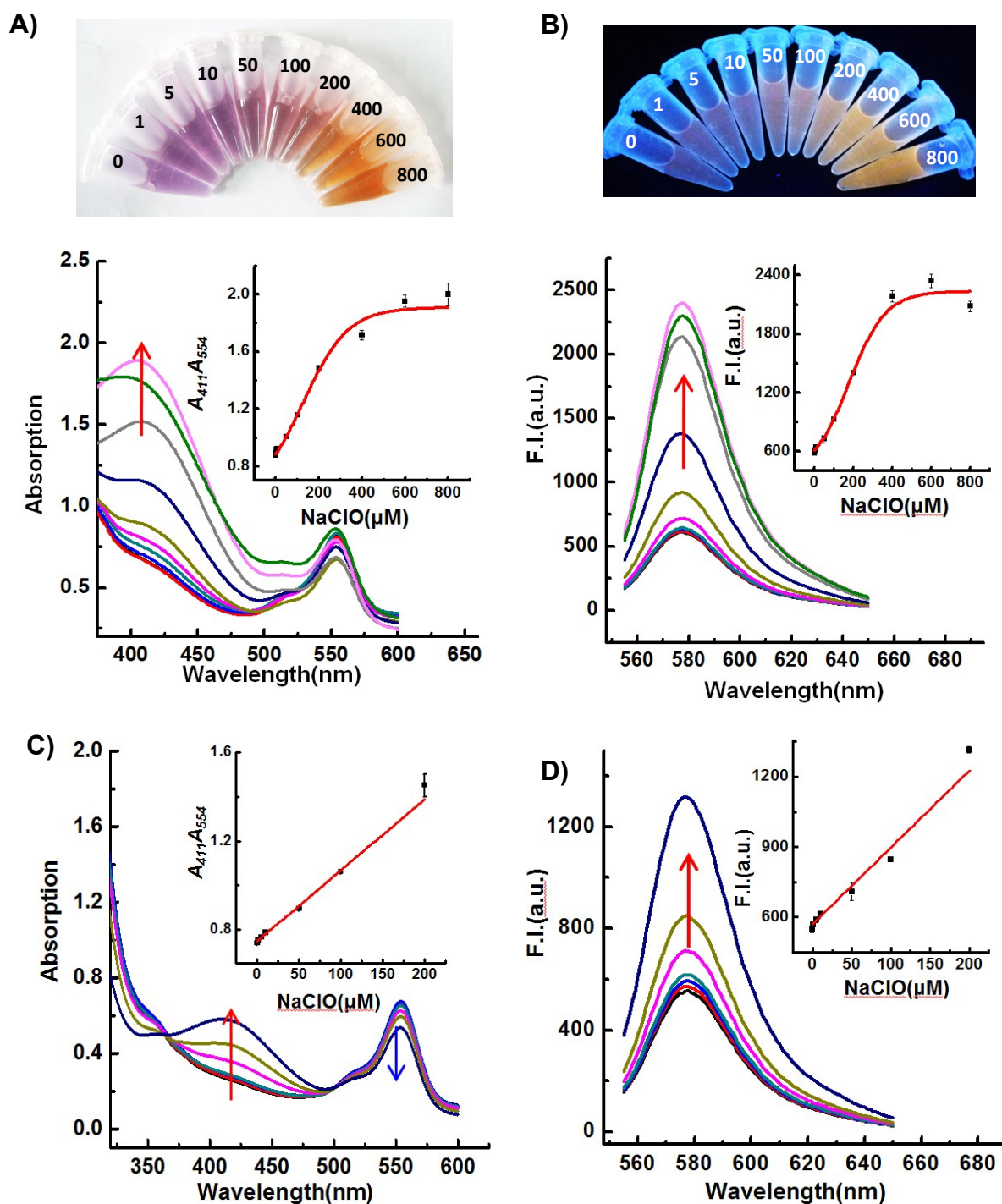


Figure S4 A) UV/Vis spectra and photographs (Upper) of the RhB@ICP nanoparticles dispersion in the presence of ClO^- . The final concentrations of ClO^- in the resulting mixtures were 0 μM , 1 μM , 5 μM , 10 μM , 50 μM , 100 μM , 200 μM , 400 μM , 600 μM , 800 μM . Inset: Plot of A_{411}/A_{554} against ClO^- concentration. B) Fluorescence spectra and photographs (Upper) of the dispersion in the presence of ClO^- . Inset: Fluorescent intensity as a function of the concentration of ClO^- . C) UV/Vis spectra of RhB@{Co(3,5-dbsq)(3,5-dbcac)(bix)}ICP

nanoparticles under different concentrations of ClO^- . Inset: Plot of A_{411}/A_{554} against ClO^- concentration. D) Fluorescence spectra of $\text{RhB}@{\text{Co}(3,5\text{-dbsq})(3,5\text{-dbcats})(\text{bix})}$ ICP nanoparticles under different concentrations of ClO^- . Inset: Fluorescent intensity as a function of the concentration of ClO^- .

As depicted in Figure S4A, after the addition of various concentrations of ClO^- to the dispersion of $\text{RhB}@{\text{Co}(3,5\text{-dbsq})(3,5\text{-dbcats})(\text{bix})}$ ICP nanoparticles (0.8mg), the color of the mixture changed from purple to orange-red in ambient light and showed a fitting range from 1 μM to 800 μM . In the linear range, with increasing the concentration of ClO^- , A_{411} increases and A_{554} decreases, however, both A_{411} and A_{554} increased when ClO^- level was high to 600 μM and 800 μM . Because such a high concentration of ClO^- caused the destruction of $\text{RhB}@{\text{Co}(3,5\text{-dbsq})(3,5\text{-dbcats})(\text{bix})}$ ICP nanoparticles completely, thus the influence on transmission light of dispersion caused by the blue shell could be ignored.